

Measurement of neutral pion pair production in two-photon collisions

K. Abe,¹⁰ I. Adachi,¹⁰ H. Aihara,⁵² K. Arinstein,¹ T. Aso,⁵⁶ V. Aulchenko,¹ T. Aushev,^{22,16}
 T. Aziz,⁴⁸ S. Bahinipati,³ A. M. Bakich,⁴⁷ V. Balagura,¹⁶ Y. Ban,³⁸ S. Banerjee,⁴⁸
 E. Barberio,²⁵ A. Bay,²² I. Bedny,¹ K. Belous,¹⁵ V. Bhardwaj,³⁷ U. Bitenc,¹⁷ S. Blyth,²⁹
 A. Bondar,¹ A. Bozek,³¹ M. Bračko,^{24,17} J. Brodzicka,¹⁰ T. E. Browder,⁹ M.-C. Chang,⁴
 P. Chang,³⁰ Y. Chao,³⁰ A. Chen,²⁸ K.-F. Chen,³⁰ W. T. Chen,²⁸ B. G. Cheon,⁸
 C.-C. Chiang,³⁰ R. Chistov,¹⁶ I.-S. Cho,⁵⁸ S.-K. Choi,⁷ Y. Choi,⁴⁶ Y. K. Choi,⁴⁶ S. Cole,⁴⁷
 J. Dalseno,²⁵ M. Danilov,¹⁶ A. Das,⁴⁸ M. Dash,⁵⁷ J. Dragic,¹⁰ A. Drutskoy,³ S. Eidelman,¹
 D. Epifanov,¹ S. Fratina,¹⁷ H. Fujii,¹⁰ M. Fujikawa,²⁷ N. Gabyshev,¹ A. Garmash,⁴⁰
 A. Go,²⁸ G. Gokhroo,⁴⁸ P. Goldenzweig,³ B. Golob,^{23,17} M. Grosse Perdekamp,^{12,41}
 H. Guler,⁹ H. Ha,¹⁹ J. Haba,¹⁰ K. Hara,²⁶ T. Hara,³⁶ Y. Hasegawa,⁴⁵ N. C. Hastings,⁵²
 K. Hayasaka,²⁶ H. Hayashii,²⁷ M. Hazumi,¹⁰ D. Heffernan,³⁶ T. Higuchi,¹⁰ L. Hinz,²²
 H. Hoedlmoser,⁹ T. Hokuue,²⁶ Y. Horii,⁵¹ Y. Hoshi,⁵⁰ K. Hoshina,⁵⁵ S. Hou,²⁸
 W.-S. Hou,³⁰ Y. B. Hsiung,³⁰ H. J. Hyun,²¹ Y. Igarashi,¹⁰ T. Iijima,²⁶ K. Ikado,²⁶
 K. Inami,²⁶ A. Ishikawa,⁴² H. Ishino,⁵³ R. Itoh,¹⁰ M. Iwabuchi,⁶ M. Iwasaki,⁵² Y. Iwasaki,¹⁰
 C. Jacoby,²² N. J. Joshi,⁴⁸ M. Kaga,²⁶ D. H. Kah,²¹ H. Kaji,²⁶ S. Kajiwara,³⁶
 H. Kakuno,⁵² J. H. Kang,⁵⁸ P. Kapusta,³¹ S. U. Kataoka,²⁷ N. Katayama,¹⁰ H. Kawai,²
 T. Kawasaki,³³ A. Kibayashi,¹⁰ H. Kichimi,¹⁰ H. J. Kim,²¹ H. O. Kim,⁴⁶ J. H. Kim,⁴⁶
 S. K. Kim,⁴⁴ Y. J. Kim,⁶ K. Kinoshita,³ S. Korpar,^{24,17} Y. Kozakai,²⁶ P. Križan,^{23,17}
 P. Krokovny,¹⁰ R. Kumar,³⁷ E. Kurihara,² A. Kusaka,⁵² A. Kuzmin,¹ Y.-J. Kwon,⁵⁸
 J. S. Lange,⁵ G. Leder,¹⁴ J. Lee,⁴⁴ J. S. Lee,⁴⁶ M. J. Lee,⁴⁴ S. E. Lee,⁴⁴ T. Lesiak,³¹
 J. Li,⁹ A. Limosani,²⁵ S.-W. Lin,³⁰ Y. Liu,⁶ D. Liventsev,¹⁶ J. MacNaughton,¹⁰
 G. Majumder,⁴⁸ F. Mandl,¹⁴ D. Marlow,⁴⁰ T. Matsumura,²⁶ A. Matyja,³¹ S. McOnie,⁴⁷
 T. Medvedeva,¹⁶ Y. Mikami,⁵¹ W. Mitaroff,¹⁴ K. Miyabayashi,²⁷ H. Miyake,³⁶ H. Miyata,³³
 Y. Miyazaki,²⁶ R. Mizuk,¹⁶ G. R. Moloney,²⁵ T. Mori,²⁶ J. Mueller,³⁹ A. Murakami,⁴²
 T. Nagamine,⁵¹ Y. Nagasaka,¹¹ Y. Nakahama,⁵² I. Nakamura,¹⁰ E. Nakano,³⁵ M. Nakao,¹⁰
 H. Nakayama,⁵² H. Nakazawa,²⁸ Z. Natkaniec,³¹ K. Neichi,⁵⁰ S. Nishida,¹⁰ K. Nishimura,⁹
 Y. Nishio,²⁶ I. Nishizawa,⁵⁴ O. Nitoh,⁵⁵ S. Noguchi,²⁷ T. Nozaki,¹⁰ A. Ogawa,⁴¹
 S. Ogawa,⁴⁹ T. Ohshima,²⁶ S. Okuno,¹⁸ S. L. Olsen,⁹ S. Ono,⁵³ W. Ostrowicz,³¹
 H. Ozaki,¹⁰ P. Pakhlov,¹⁶ G. Pakhlova,¹⁶ H. Palka,³¹ C. W. Park,⁴⁶ H. Park,²¹
 K. S. Park,⁴⁶ N. Parslow,⁴⁷ L. S. Peak,⁴⁷ M. Pernicka,¹⁴ R. Pestotnik,¹⁷ M. Peters,⁹
 L. E. Piilonen,⁵⁷ A. Poluektov,¹ J. Rorie,⁹ M. Rozanska,³¹ H. Sahoo,⁹ Y. Sakai,¹⁰
 H. Sakaue,³⁵ N. Sasao,²⁰ T. R. Sarangi,⁶ N. Satoyama,⁴⁵ K. Sayeed,³ T. Schietinger,²²
 O. Schneider,²² P. Schönmeier,⁵¹ J. Schümman,¹⁰ C. Schwanda,¹⁴ A. J. Schwartz,³
 R. Seidl,^{12,41} A. Sekiya,²⁷ K. Senyo,²⁶ M. E. Sevier,²⁵ L. Shang,¹³ M. Shapkin,¹⁵
 C. P. Shen,¹³ H. Shibuya,⁴⁹ S. Shinomiya,³⁶ J.-G. Shiu,³⁰ B. Shwartz,¹ J. B. Singh,³⁷
 A. Sokolov,¹⁵ E. Solovieva,¹⁶ A. Somov,³ S. Stanič,³⁴ M. Starič,¹⁷ J. Stypula,³¹
 A. Sugiyama,⁴² K. Sumisawa,¹⁰ T. Sumiyoshi,⁵⁴ S. Suzuki,⁴² S. Y. Suzuki,¹⁰ O. Tajima,¹⁰
 F. Takasaki,¹⁰ K. Tamai,¹⁰ N. Tamura,³³ M. Tanaka,¹⁰ N. Taniguchi,²⁰ G. N. Taylor,²⁵
 Y. Teramoto,³⁵ I. Tikhomirov,¹⁶ K. Trabelsi,¹⁰ Y. F. Tse,²⁵ T. Tsuboyama,¹⁰ K. Uchida,⁹

Y. Uchida,⁶ S. Uehara,¹⁰ K. Ueno,³⁰ T. Uglov,¹⁶ Y. Unno,⁸ S. Uno,¹⁰ P. Urquijo,²⁵
Y. Ushiroda,¹⁰ Y. Usov,¹ G. Varner,⁹ K. E. Varvell,⁴⁷ K. Vervink,²² S. Villa,²²
A. Vinokurova,¹ C. C. Wang,³⁰ C. H. Wang,²⁹ J. Wang,³⁸ M.-Z. Wang,³⁰ P. Wang,¹³
X. L. Wang,¹³ M. Watanabe,³³ Y. Watanabe,¹⁸ R. Wedd,²⁵ J. Wicht,²² L. Widhalm,¹⁴
J. Wiechczynski,³¹ E. Won,¹⁹ B. D. Yabsley,⁴⁷ A. Yamaguchi,⁵¹ H. Yamamoto,⁵¹
M. Yamaoka,²⁶ Y. Yamashita,³² M. Yamauchi,¹⁰ C. Z. Yuan,¹³ Y. Yusa,⁵⁷ C. C. Zhang,¹³
L. M. Zhang,⁴³ Z. P. Zhang,⁴³ V. Zhilich,¹ V. Zhulanov,¹ A. Zupanc,¹⁷ and N. Zwahlen²²

(The Belle Collaboration)

¹*Budker Institute of Nuclear Physics, Novosibirsk*

²*Chiba University, Chiba*

³*University of Cincinnati, Cincinnati, Ohio 45221*

⁴*Department of Physics, Fu Jen Catholic University, Taipei*

⁵*Justus-Liebig-Universität Gießen, Gießen*

⁶*The Graduate University for Advanced Studies, Hayama*

⁷*Gyeongsang National University, Chinju*

⁸*Hanyang University, Seoul*

⁹*University of Hawaii, Honolulu, Hawaii 96822*

¹⁰*High Energy Accelerator Research Organization (KEK), Tsukuba*

¹¹*Hiroshima Institute of Technology, Hiroshima*

¹²*University of Illinois at Urbana-Champaign, Urbana, Illinois 61801*

¹³*Institute of High Energy Physics,*

Chinese Academy of Sciences, Beijing

¹⁴*Institute of High Energy Physics, Vienna*

¹⁵*Institute of High Energy Physics, Protvino*

¹⁶*Institute for Theoretical and Experimental Physics, Moscow*

¹⁷*J. Stefan Institute, Ljubljana*

¹⁸*Kanagawa University, Yokohama*

¹⁹*Korea University, Seoul*

²⁰*Kyoto University, Kyoto*

²¹*Kyungpook National University, Taegu*

²²*École Polytechnique Fédérale de Lausanne (EPFL), Lausanne*

²³*University of Ljubljana, Ljubljana*

²⁴*University of Maribor, Maribor*

²⁵*University of Melbourne, School of Physics, Victoria 3010*

²⁶*Nagoya University, Nagoya*

²⁷*Nara Women's University, Nara*

²⁸*National Central University, Chung-li*

²⁹*National United University, Miao Li*

³⁰*Department of Physics, National Taiwan University, Taipei*

³¹*H. Niewodniczanski Institute of Nuclear Physics, Krakow*

³²*Nippon Dental University, Niigata*

³³*Niigata University, Niigata*

³⁴*University of Nova Gorica, Nova Gorica*

³⁵*Osaka City University, Osaka*

³⁶*Osaka University, Osaka*

³⁷*Panjab University, Chandigarh*

- ³⁸*Peking University, Beijing*
- ³⁹*University of Pittsburgh, Pittsburgh, Pennsylvania 15260*
- ⁴⁰*Princeton University, Princeton, New Jersey 08544*
- ⁴¹*RIKEN BNL Research Center, Upton, New York 11973*
- ⁴²*Saga University, Saga*
- ⁴³*University of Science and Technology of China, Hefei*
- ⁴⁴*Seoul National University, Seoul*
- ⁴⁵*Shinshu University, Nagano*
- ⁴⁶*Sungkyunkwan University, Suwon*
- ⁴⁷*University of Sydney, Sydney, New South Wales*
- ⁴⁸*Tata Institute of Fundamental Research, Mumbai*
- ⁴⁹*Toho University, Funabashi*
- ⁵⁰*Tohoku Gakuin University, Tagajo*
- ⁵¹*Tohoku University, Sendai*
- ⁵²*Department of Physics, University of Tokyo, Tokyo*
- ⁵³*Tokyo Institute of Technology, Tokyo*
- ⁵⁴*Tokyo Metropolitan University, Tokyo*
- ⁵⁵*Tokyo University of Agriculture and Technology, Tokyo*
- ⁵⁶*Toyama National College of Maritime Technology, Toyama*
- ⁵⁷*Virginia Polytechnic Institute and State University, Blacksburg, Virginia 24061*
- ⁵⁸*Yonsei University, Seoul*

Abstract

The differential cross section of the process $\gamma\gamma \rightarrow \pi^0\pi^0$ has been measured in the kinematical range $0.6 \text{ GeV} < W < 4.0 \text{ GeV}$ and $|\cos\theta^*| < 0.8$ in energy and pion scattering angle, respectively, in the $\gamma\gamma$ center-of-mass system. We find at least four resonant structures including a peak from $f_0(980)$. In addition, there is evidence for χ_{c0} production. We also make a preliminary discussion of the angular dependence and cross section ratio to $\gamma\gamma \rightarrow \pi^+\pi^-$.

PACS numbers: 13.20.Gd, 13.60.Le, 13.66.Bc, 14.40.Cs, 14.40.Gx

I. INTRODUCTION

Measurements of exclusive hadronic final states in two-photon collisions provide valuable information concerning the physics of light and heavy-quark resonances, perturbative and non-perturbative QCD and hadron-production mechanisms. So far, we have measured the production cross sections of charged-pion pairs [1, 2], charged and neutral-kaon pairs [2, 3], and proton-antiproton pairs [4]. We have also analyzed D -meson-pair production to search for a new charmonium state [5].

In this report, we show an analysis of neutral-pion pair production in two-photon processes. The motivation for this study is essentially the same as that for the charged-pion pair case. But the two processes are physically different and independent; we cannot predict very precisely what happens in one by measuring only the other.

In the low energy region ($W < 1.0$ GeV), it is expected that the difference of meson electric charges plays an essential role in the difference between the $\pi^+\pi^-$ and $\pi^0\pi^0$ cross sections. The predictions are not easy because of non-perturbative effects. In the intermediate energy range ($1.0 < W < 2.4$ GeV), the formation of meson resonances decaying to $\pi\pi$ is the dominant contribution. For ordinary $q\bar{q}$ mesons conserving isospin in decays to $\pi\pi$, the only allowed $I^G J^{PC}$ states produced by two photons are $0^+(\text{even})^{++}$, that is, $f_{J=\text{even}}$ mesons. The ratio of the f -meson's branching fractions, $\mathcal{B}(f \rightarrow \pi^0\pi^0)/\mathcal{B}(f \rightarrow \pi^+\pi^-)$ is 1/2 from isospin invariance. But, interference of the resonance with the continuum component which cannot be precisely calculated distorts the ratio even near the resonant peaks. The $\pi^0\pi^0$ channel has an advantage in the study of resonances, since a smaller contribution from the continuum is expected in it than in the $\pi^+\pi^-$ channel.

For higher energies, we can invoke a quark model. In the leading order calculations [6, 7] which take into account spin correlation between quarks, the $\pi^0\pi^0$ cross section is predicted to be much smaller than that of $\pi^+\pi^-$, and the cross section ratio of $\pi^0\pi^0$ to $\pi^+\pi^-$ is around 0.03-0.06. However, higher-order or non-perturbative QCD effects can modify the ratio. For example, the handbag model which considers soft hadron exchange predicts the same amplitude for the two processes, and this ratio becomes 0.5 [8]. Analyses of energy and angular distributions of the cross sections are essential for determining properties of the observed resonances and for testing the validity of QCD models.

We present preliminary results of the measurement of the differential cross section, $d\sigma/d|\cos\theta^*|$, for the process $\gamma\gamma \rightarrow \pi^0\pi^0$ in a wide two-photon center-of-mass (c.m.) energy (W) range from 0.6 to 4.0 GeV, and a c.m. angular range, $|\cos\theta^*| < 0.8$. (Although we do not need to put the absolute-value symbol for $\cos\theta^*$ for the present channel where the identical particle pairs appear in both initial and final states, we follow the usual convention of the two-photon differential cross section to avoid unnecessary confusion.) Our data sample is by several hundred times larger than in previous experiments [9, 10].

II. EXPERIMENTAL APPARATUS AND TRIGGER

We use a data sample that corresponds to an integrated luminosity of 95 fb^{-1} recorded with the Belle detector at the KEKB asymmetric-energy e^+e^- collider [11]. The energy of the accelerator was set at 10.58 GeV (83 fb^{-1}), 10.52 GeV (9 fb^{-1}), 10.36 GeV ($\Upsilon(3S)$ runs, 2.9 fb^{-1}) and 10.30 GeV (0.3 fb^{-1}), in the c.m. energy of the e^+e^- beams. The difference of the two-photon flux (luminosity function) in the measured W regions due to the different beam energies is very small (a few percent at maximum), and the fraction of integrated

luminosity of the runs with the lower beam energies is very small. We therefore combine the results for different beam energies. The effect on the cross section deviation is less than 0.5%. The analysis is made in the “zero-tag” mode, where neither the recoil electron nor positron is detected. We restrict the virtuality of the incident photons to be small by imposing strict transverse-momentum balance with respect to the beam axis for the final-state hadronic system.

A comprehensive description of the Belle detector is given elsewhere [12]. We mention here only those detector components which are essential for the present measurement. Charged tracks are reconstructed from hit information in a central drift chamber (CDC) located in a uniform 1.5 T solenoidal magnetic field. The detector solenoid is along the z axis which points in the direction opposite to that of the positron beam. The CDC and a silicon vertex detector measure the longitudinal and transverse momentum components (along the z axis and in the $r\varphi$ plane, respectively). Photon detection and energy measurements are performed with a CsI(Tl) electromagnetic calorimeter (ECL).

In the present measurement, we require that there be no reconstructed tracks coming from the vicinity of the nominal collision point. Therefore, the CDC is used for vetoing events with track(s). Photons from decays of two neutral pions are detected and their momentum vectors are measured by the ECL.

Signals from the ECL are used to trigger the signal events. The conditions of the ECL trigger are as follows: The ECL total energy deposit in the triggerable acceptance region (see the next subsection) is greater than 1.15 GeV (the ‘HiE’ trigger), or, the number of the ECL clusters counted according to the energy threshold at 110 MeV for segments of the ECL is four or greater (the ‘Clst4’ trigger). The above energy thresholds are determined from the experimental data from a study of the correlations between the two triggers. No software filterings are applied for triggering events by either or both of the two ECL triggers.

III. EVENT SELECTION

The selection conditions for signal candidates of $\gamma\gamma \rightarrow \pi^0\pi^0$ are as follows: All the variables in the criteria (1)-(5) are measured in the laboratory frame; (1) there is no good track that satisfies $dr < 5$ cm, $|dz| < 5$ cm and $p_t > 0.1$ GeV/ c , where dr and dz are the radial and axial distances, respectively, of the closest approach (as seen in the $r\varphi$ plane) to the nominal collision point, and the p_t is the transverse momentum measured in the laboratory frame with respect to the z axis; (2) the events are triggered by the HiE or Clst4 triggers; (3) there are two or more photons whose energy is greater than 100 MeV; (4) there are just two π^0 's, each having transverse momentum greater than 0.15 GeV/ c , and each of the decay-product photons has energy greater than 70 MeV, where the π^0 is reconstructed from two photons and is selected with a χ^2 value of a mass constraint fit; (5) the total energy deposit in ECL is smaller than 5.7 GeV.

Then, the transverse momentum in the e^+e^- c.m. frame ($|\Sigma\mathbf{p}_t^*|$) of the two-pion system is calculated. For further analysis, (6) we use events with $|\Sigma\mathbf{p}_t^*| < 50$ MeV/ c as the signal candidates.

In order to reduce uncertainty from the efficiency of the hardware ECL triggers, we set offline selection criteria which emulate the hardware trigger conditions as follows: (7) the ECL energy sum within the triggerable region is greater than 1.25 GeV, *or* all the four photons composing the two π^0 are contained in the triggerable acceptance region. Here, we define the triggerable acceptance region as the polar-angle range in the laboratory system

$17.0^\circ < \theta < 128.7^\circ$.

IV. SIGNAL CANDIDATES AND BACKGROUNDS

A. Yield distribution of the signal candidates

We derive the c.m. energy W of the two-photon collision from the invariant mass of the two neutral pion system. We calculate cosine of the scattering angle of π^0 in the $\gamma\gamma$ c.m. frame, $|\cos\theta^*|$ for each event. We use the e^+e^- collision axis in the e^+e^- c.m. frame as the reference of the polar angle as an approximation, because we do not know the exact $\gamma\gamma$ collision axis.

The two-dimensional yield distribution of the selected events is shown by the lego plot in Fig. 1. The W distribution with $|\cos\theta^*| < 0.8$ is shown in Fig. 2(a). We find at least four resonant structures: clear peaks from $f_0(980)$ near 0.98 GeV and $f_2(1270)$ near 1.25 GeV, and broad structures near 1.65 GeV and near 1.95 GeV. Figure 2(b) is an enlarged view of the charmonium region for $|\cos\theta^*| < 0.4$, where we see some hints of charmonium contributions in the χ_{c0} (~ 3.40 GeV) and χ_{c2} (~ 3.55 GeV) mass region.

B. Background subtraction

We study the p_t -balance distribution, i.e., the event distribution in $|\Sigma\mathbf{p}_t^*|$ to separate the signal and background components. The signal Monte Carlo (MC) events show that the signal component peaks around 10-20 MeV/ c in this distribution. In the experimental data, however, in addition to such a signal component, we find some contribution from the p_t -unbalanced components in the low- W region. The source of such p_t -unbalanced components, in general, is considered to be non-exclusive processes such as $\pi^0\pi^0\pi^0$ etc. But, in the present case, the background found in the experimental data is very large only in the low W region where the $\pi^0\pi^0\pi^0$ contribution is expected to be much smaller than $\pi^0\pi^0$ in two-photon collisions. (Note that a C -parity odd system cannot go to $\pi^0\pi^0$.) We believe that the backgrounds are dominated by beam-background photons (or neutral pions from secondary interactions) or spurious hits in the detector.

Figures 3 (a) and (b) show the p_t -balance distributions in the low W region. With the fit described below, we separate the signal components from the background. In the intermediate or higher energy regions, the backgrounds are less than 1%, buried under the $f_2(1270)$ peak (Fig. 3(c)), or we do not see any detectable p_t -unbalanced components within the statistical errors (as shown in Fig. 3(d)). Even at the highest energy $3.6 \text{ GeV} < W < 4.0 \text{ GeV}$, $|\cos\theta^*| < 0.4$, we find no visible contamination from the background.

A fit to the p_t -balance distribution is made to separate the signal and background components for the W region below 1.2 GeV. The fit function is a sum of the signal component and the background component. The signal component is taken as an empirical function reproducing the shape of the signal MC, $y = Ax/(x^{2.1} + B + Cx)$, where ($x \equiv |\Sigma\mathbf{p}_t^*|$, A , B and C are the fitting parameters, and y is the distribution). This function has a peak at $x = (\frac{B}{1.1})^{\frac{1}{2.1}}$ and vanishes at $x = 0$ and infinite x . The shape of the background is taken as a linear function $y = ax$ for $x < 0.05 \text{ GeV}/c$ which is smoothly connected to a quadratic function above $x > 0.05 \text{ GeV}/c$.

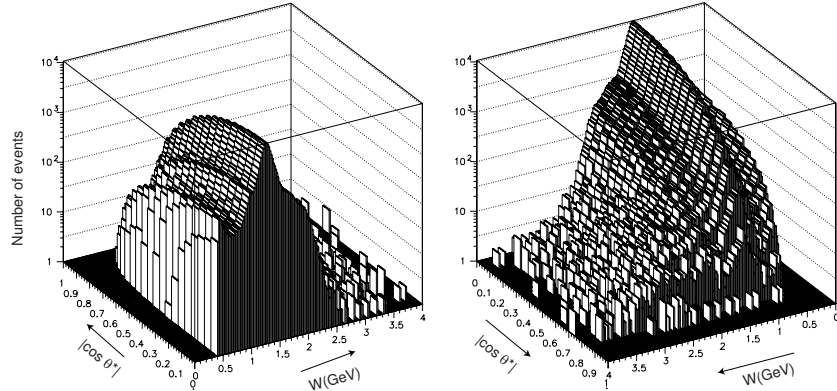


FIG. 1: The two-dimensional distribution of the experimental $\pi^0\pi^0$ candidates. The same distribution is viewed from two different directions.

The background yields obtained from the fits are fitted to a smooth two-dimensional function of $(W, |\cos\theta^*|)$ in order to minimize statistical fluctuations. Then, the backgrounds are subtracted from the experimental yield distribution. The background yields integrated over the angle is shown in Fig. 2(a). We omit the data points in the small-angle ($|\cos\theta^*| > 0.6$) region in $W < 0.72$ GeV, because there the background dominates the yield.

C. Unfolding the W distributions

We estimate the invariant-mass resolutions from studies of the signal-MC and experimental events. We find that the MC events show a relative invariant-mass resolution of 1.4%, which is almost constant in the whole W region of the present measurement. The momentum resolution of π^0 is known to be worse by about 15% in the experimental data than in MC from a study of the p_t -balance distributions (described in Sect. V). Moreover, the distribution of the MC is asymmetric; it has a longer tail on the lower mass side.

An asymmetric Gaussian function with standard deviations of $1.9\%W$ and $1.3\%W$ on the lower and higher sides of the peak, respectively, is used and approximates the smearing reasonably well.

We calibrate the experimental energy scale and invariant-mass distribution using the $\gamma\gamma$ invariant mass from experimental samples of $\eta' \rightarrow \gamma\gamma$ from two-photon processes. The peak position is consistent with the nominal mass of η' with an accuracy better than 0.2%.

This invariant-mass resolution is comparable to or larger than the W bin width (20 MeV) used in Figs. (1) and (2). We made an unfolding of the invariant-mass distribution in each $|\cos\theta^*|$ bin separately, to correct for migrations of signal yields between different W bins, based on the smearing function of the above asymmetric Gaussian shape. The migration in the $|\cos\theta^*|$ direction is expected to be small and is neglected.

The unfolding is made using the Singular Value Decomposition (SVD) algorithm [13] in the yield level, and is applied so as to reproduce the corrected W distribution in the 0.9 - 2.4 GeV region, using data at observed W between 0.72 and 3.0 GeV. For lower energies, $W < 0.9$ GeV, the effect of the migration is expected to be small because of the smaller invariant-mass resolution compared with the bin width. For higher energies, $W > 2.4$ GeV, where the statistics is relatively low and the unfolding would enlarge the errors, we rebin the result with a bin width of 100 MeV, instead of unfolding, as described in Sect. IV.C.

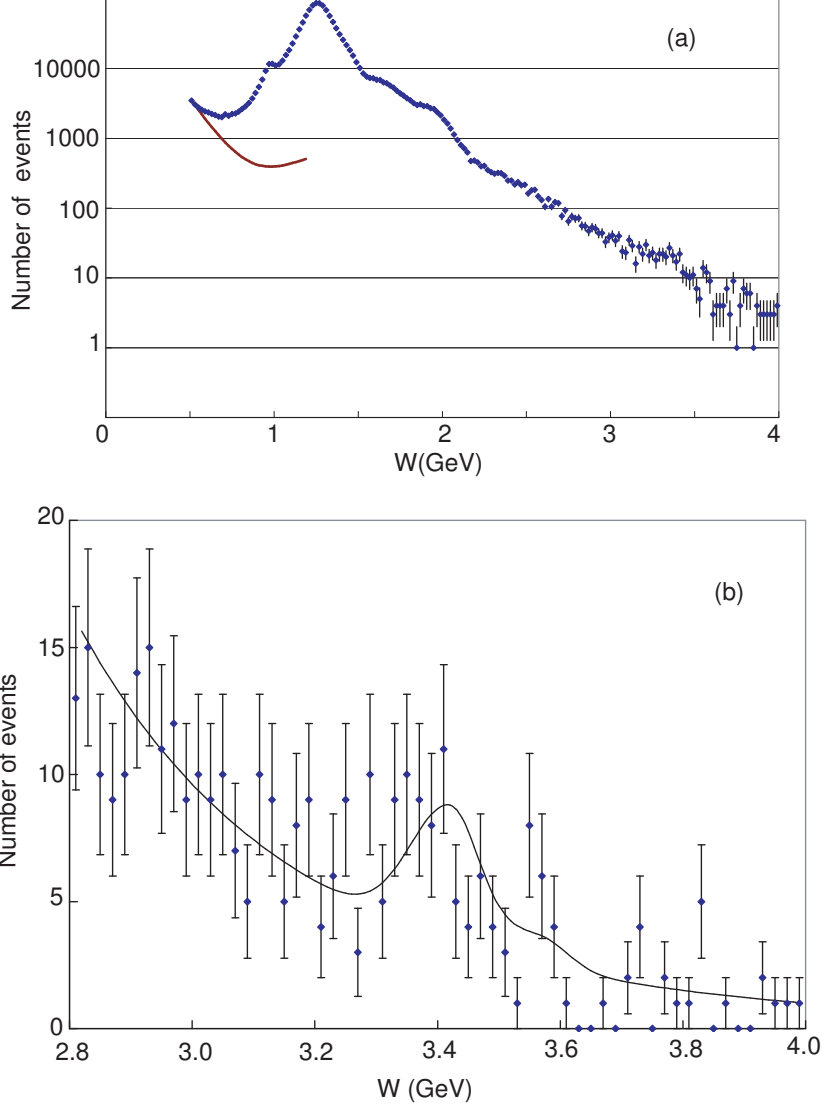


FIG. 2: The W distribution of the candidate events. (a) $|\cos \theta^*| < 0.8$. The curve is an estimate of backgrounds from events with p_t imbalance. (b) $|\cos \theta^*| < 0.4$, near the charmonium region. The curve is the fit described in Sect. VIII.

Distributions before and after the unfolding for a typical angular bin ($|\cos \theta^*| = 0.225$) are shown in Fig. 4.

V. DETERMINATION OF EFFICIENCY

We determine the trigger efficiency for signal events using the detector and trigger simulators applied to the signal MC events.

The signal MC events for $e^+e^- \rightarrow e^+e^-\pi^0\pi^0$ are generated using TREPS code [14] for the trigger efficiency study at 27 fixed W points between 0.5 and 4.1 GeV, isotropic in $|\cos \theta^*|$. The angular distribution at the generator level does not play a role for the efficiency determination, because we calculate the efficiencies separately in each $|\cos \theta^*|$ bin with width 0.05. 5×10^4 events are generated at each W point.

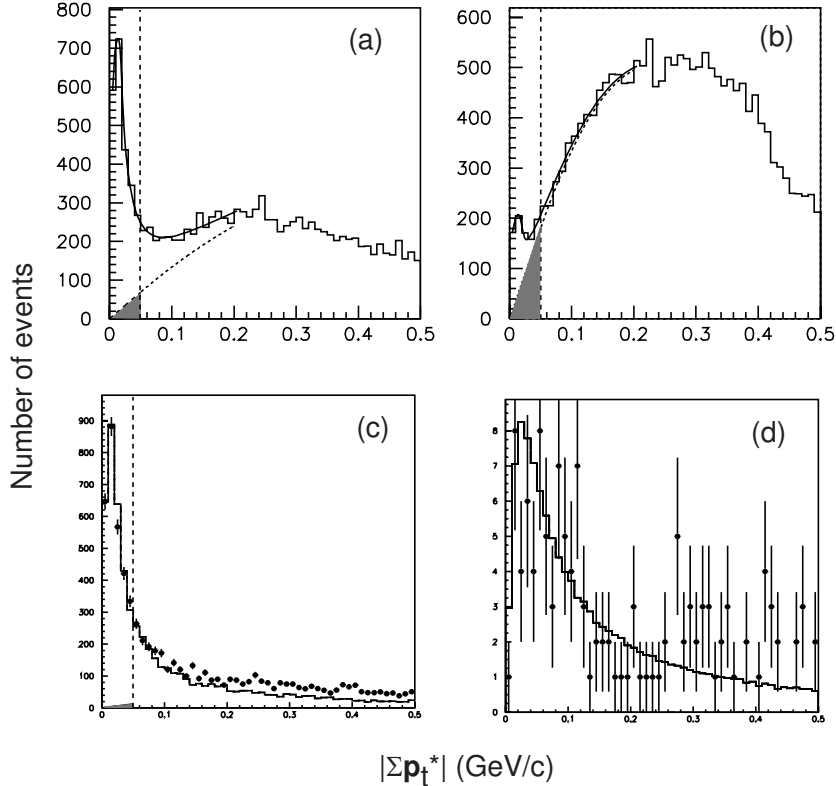


FIG. 3: The distribution of imbalance in p_t for candidate events. (a) In the bin centered at $W = 0.90$ GeV and $|\cos \theta^*| = 0.05$ (The bin width is 0.04 GeV and 0.1 in the W and $|\cos \theta^*|$ directions, respectively, in (a)-(c).), the experimental distribution (histogram) is fitted with the sum of signal and background components (curves). The grey region shows the estimated background contamination in the signal region. (b) $W = 0.66$ GeV, same as in (a) for the others. (c) In the bin of $W = 1.18$ GeV, $|\cos \theta^*| = 0.65$, the experimental distribution (dots with error bars) is compared with the signal MC (histogram). The grey region shows the estimated background contaminating the signal region obtained from the fit. (d) For $3.6 < W < 4.0$ GeV and $|\cos \theta^*| < 0.4$, the experimental distribution (dots with error bars) is compared with the signal MC (histogram).

To minimize statistical fluctuation in the MC, we fit the numerical results of the trigger efficiency to a two-dimensional empirical function in $(W, |\cos \theta^*|)$. The W dependences are shown in Fig. 5 for two typical angular bins. We find that the trigger efficiency is almost flat and close to 100% for the region W above 1.3 GeV. The angular dependence is rather small.

Separately, we generated signal MC events at 48 W points in the same W region with 10^5 events at each value of W , for the acceptance calculations. Here we call the efficiency of the selections not including the hardware trigger “acceptance”; the net efficiency is a product of the trigger efficiency and the acceptance. The determined acceptance from the MC events is fitted by a smooth two-dimensional function of $(W, |\cos \theta^*|)$ (Fig. 6). It is about 11% at maximum and gets smaller (down to around 1%) at lower W or smaller c.m. angle (larger $|\cos \theta^*|$).

The acceptance calculated using the signal MC events is corrected for a systematic difference found between the peak widths in the p_t -balance distributions of the experimental

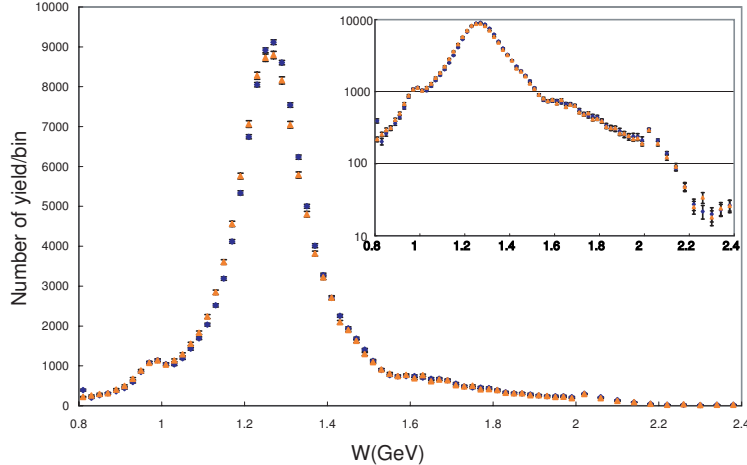


FIG. 4: Invariant mass distributions of the yield in each bin before (orange colored triangles) and after (dark-blue diamonds) the unfolding, at $|\cos \theta^*| = 0.225$. The inset shows a logarithmic plot of the same distribution. The bin width is different for the regions W below and above 2.0 GeV.

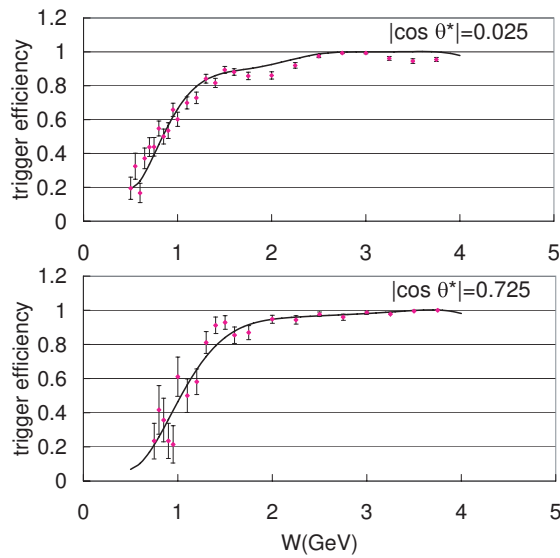


FIG. 5: The W dependence of the trigger efficiency for two angular bins. The curves are the fit to parameterize it.

data and the MC, which could affect the acceptance through the $|\Sigma \mathbf{p}_t^*|$ cut. It originates from a difference in the momentum resolution for π^0 between data and MC. We find that the peak position of the experimental data in the distribution is 10% to 20% higher than the MC expectation, depending on W and $|\cos \theta^*|$. The correction factor ranges from 0.90 to 0.95.

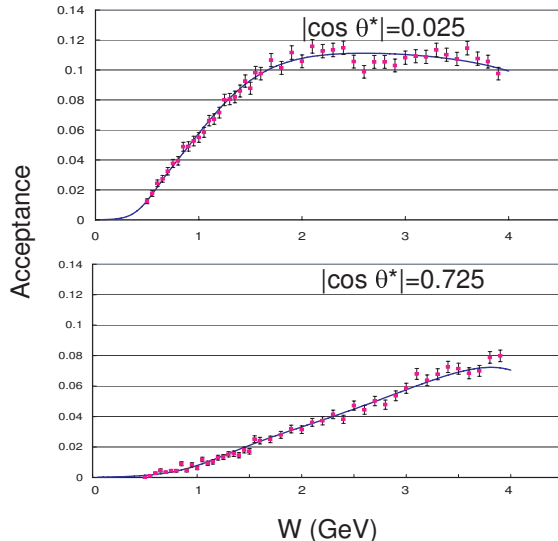


FIG. 6: The W dependence of the acceptance for two angular bins. The curves are the fit to parameterize it. No correction for the π^0 momentum resolution is included.

VI. CROSS SECTION CALCULATION

The differential cross section for each $(W, |\cos\theta^*|)$ point is derived by the following formula:

$$\frac{d\sigma}{d|\cos\theta^*|} = \frac{\Delta Y - \Delta B}{\Delta W \Delta|\cos\theta^*| \int \mathcal{L} dt L_{\gamma\gamma}(W) \eta_{\text{trg}} \eta_{\text{acc}}}$$

where ΔY and ΔB are the signal yield and the estimated p_t -unbalanced background in the bin, ΔW and $\Delta|\cos\theta^*|$ are the bin widths, $\int \mathcal{L} dt$ and $L_{\gamma\gamma}(W)$ are the integrated luminosity and two-photon luminosity function calculated by TREPS, respectively, and η_{trg} and η_{acc} are the trigger efficiency and the acceptance, respectively, the latter including the correction described in the previous section.

Figures 7(a) and (b) show the W dependence of the cross section integrated over $|\cos\theta^*| < 0.8$ and $|\cos\theta^*| < 0.6$, respectively. They are obtained by simply adding $d\sigma/d|\cos\theta^*| \cdot \Delta|\cos\theta^*|$ over the corresponding angular bins.

The data points for $0.9 \text{ GeV} < W < 2.4 \text{ GeV}$ are the unfolded results with the bin widths $\Delta W = 0.02 \text{ GeV}$ (0.04 GeV) for W above (below) 2.0 GeV . For the data points above 2.4 GeV , we average five data points each with a bin width of 0.02 GeV and get results for every 0.1 GeV at W . We have removed the bins in the range $3.3 \text{ GeV} < W < 3.6 \text{ GeV}$, because we cannot separate the components of the χ_{c0} , χ_{c2} and the continuum in a model-independent way due to a finite mass resolution and insufficient statistics in the measurement.

We show the angular dependence of the differential cross section at several W points in Fig. 8.

It is noted that the cross section results after the unfolding are no longer independent of each other in the neighboring bins, in both central values and size of errors.

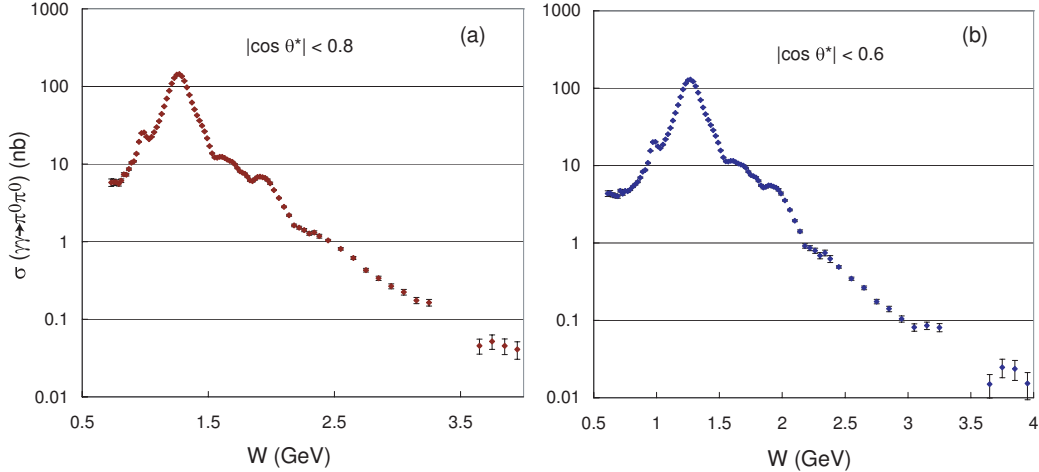


FIG. 7: The cross section results integrated in the angular regions (a) $|\cos\theta^*| < 0.8$ and (b) $|\cos\theta^*| < 0.6$ after the unfolding and rebinning.

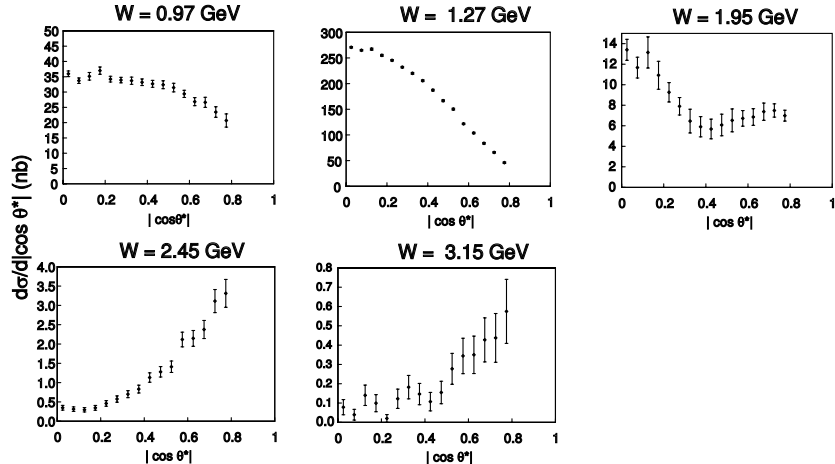


FIG. 8: The differential cross sections for five selected W points, 0.97 GeV, 1.27 GeV, 1.95 GeV, 2.45 GeV and 3.15 GeV. The results of the first three W points are after the unfolding.

VII. SYSTEMATIC ERRORS

We summarize the evaluation of the systematic errors for $\sigma(|\cos\theta^*| < 0.8)$ ($\sigma(|\cos\theta^*| < 0.6)$ with $W < 0.72$ GeV) for each W point. They come from the following major error sources:

Trigger efficiency: The systematic error of the Clst4 trigger is assigned as 2/3 of the difference of the efficiencies with the different threshold assumptions for the ECL cluster – 110 MeV and 100 MeV – set in the trigger simulator for the energy region $W < 2.5$ GeV. Separately, we take the uncertainty in the HiE trigger efficiency as 4% for the whole W region. The systematic errors from the two triggers are added in quadrature. This systematic error is large in the low W region, 20%-30% for $W < 0.8$ GeV.

The reconstruction efficiency: 6% for two pions.

The p_t -balance cut: 3%-5%. One half of the correction size discussed in Sect. V.

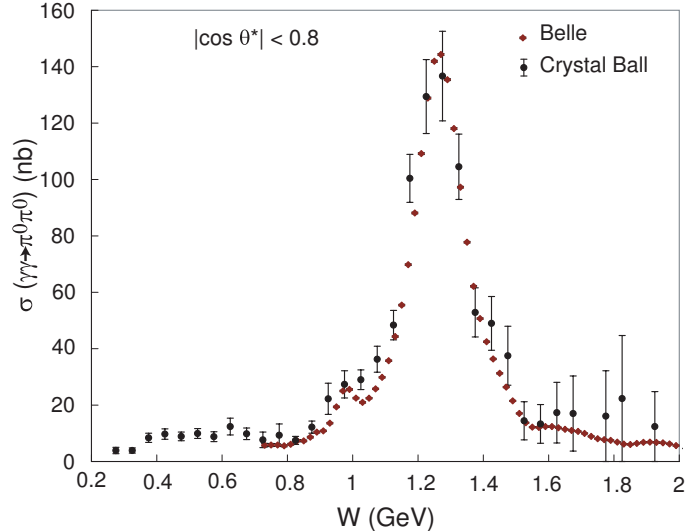


FIG. 9: The cross section results integrated over the angular regions $|\cos \theta^*| < 0.8$ compared with the previous measurement from the Crystal Ball [10].

Background subtraction: 20% of the size of the subtracted component is assigned as the error from this source. In the W region where the background subtraction is not applied ($W > 1.2$ GeV), we neglect the error for $1.2 \text{ GeV} < W < 1.5 \text{ GeV}$, or assign 3% for $W > 1.5$ GeV, considering an upper limit of the background contamination expected from the p_t -balance distributions.

Luminosity function 4-5%. 4% (5%) for $W < (>) 3.0$ GeV.

The total systematic error is 9% in the intermediate W region, $1.05 \text{ GeV} < W < 2.7 \text{ GeV}$. It is much larger for lower W , 15% at $W = 0.85$ GeV, 30% at $W = 0.70$ GeV and 55% at $W = 0.61$ GeV. The error is dominated by the background subtraction for low W . For higher W , the systematic error is rather stable, 10%-11% for $2.7 \text{ GeV} < W < 4.0$ GeV.

VIII. DISCUSSION

We compare our results with the previous measurements by Crystal Ball at DORIS II [10] (Fig. 9). The agreement is fairly good. The error bars from the two experiments are statistical only, and the systematic errors (7% (11%) for $W > (<) 0.8$ GeV for the Crystal Ball results) should also be considered in the comparison. The present measurement has several hundred times more statistics than the Crystal Ball measurement.

We find prominent resonant structures near 0.98 GeV and 1.27 GeV. They are from $f_0(980)$ and $f_2(1270)$, respectively and are observed also in the $\gamma\gamma \rightarrow \pi^+\pi^-$ process [1]. It is for the first time that the $f_0(980)$ is observed as a clear peak in $\gamma\gamma \rightarrow \pi^0\pi^0$. We find clear evidence for rather broad peaks at 1.65 GeV and 1.95 GeV. For these, any quick assignment to well known states is not easy. In addition, we find a hint of a possible inflection point near 1.4 GeV and a structure in the mass region of two charmonium states χ_{c0} and χ_{c2} . The structures above found in the 1.2 - 2.1 GeV region are somewhat similar to the distribution observed in the $\pi^0\pi^0$ spectrum from the $\pi^-p \rightarrow \pi^0\pi^0n$ experiment, GAMS [15].

We fit the yield distribution in the range $2.8 \text{ GeV} < W < 4.0 \text{ GeV}$ and $|\cos \theta^*| < 0.4$ including the contribution from the χ_{c0} and χ_{c2} charmonia with a binned maximum-likelihood

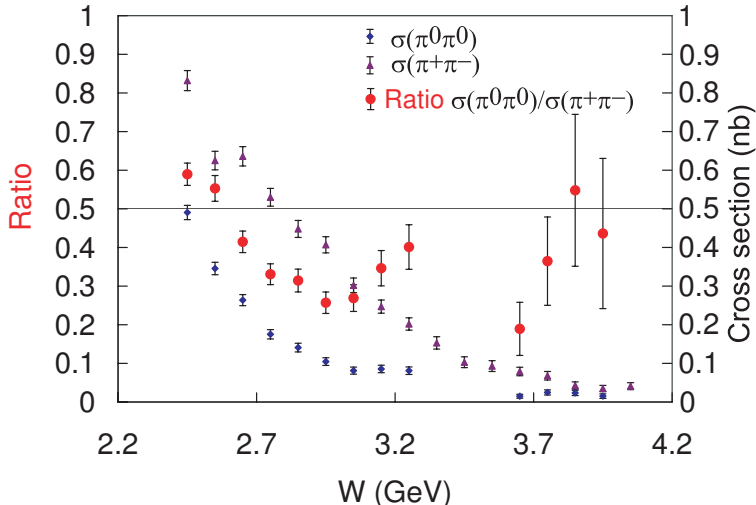


FIG. 10: The cross sections of the $\gamma\gamma \rightarrow \pi^0\pi^0$ and $\gamma\gamma \rightarrow \pi^+\pi^-$ reactions for $|\cos\theta^*| < 0.6$. The blue closed circle and the violet triangles are the cross sections of the two reactions in units of nb. The red closed circle is the ratio. The error bars are statistical only.

method. The fit is shown in Fig. 2(b). We take into account the finite invariant-mass resolution effect introduced in the last section in the fit. We have fixed the nominal masses and the width of χ_{c0} to the world averages [16] (we neglect the width of χ_{c2}). The background component is assumed to have the shape of $\sim W^{-n}$.

From the fit, we find the yields 35.3 ± 9.2 events and 8.2 ± 6.4 events for χ_{c0} and χ_{c2} , respectively. These yields provide the products of the two-photon decay widths and the branching fractions, $\Gamma_{\gamma\gamma}(\chi_{cJ})\mathcal{B}(\chi_{cJ} \rightarrow \pi^0\pi^0) = 8.4 \pm 2.2(stat.) \pm 0.8(syst.)$ eV and $0.29 \pm 0.23 \pm 0.03$ eV, for χ_{c0} and χ_{c2} , respectively. The former and latter provide evidence for the $\gamma\gamma \rightarrow \chi_{c0} \rightarrow \pi^0\pi^0$ signal at the 4.5σ level and an upper limit at the 90% C.L., $\Gamma_{\gamma\gamma}(\chi_{c2})\mathcal{B}(\chi_{c2} \rightarrow \pi^0\pi^0) < 0.75$ eV which is obtained from the yield where the two times the log-likelihood of the fit is smaller by $(1.64)^2$ than that of the best fit, respectively. The above central values show good agreement with the world averages of $\Gamma_{\gamma\gamma}(\chi_{cJ})\mathcal{B}$ measured in the $\chi_{cJ} \rightarrow \pi^+\pi^-$ process [16], considering isospin invariance (apply $\pi^0\pi^0 : \pi\pi = 1 : 3$ to the branching fractions), which includes the Belle measurements of the process $\gamma\gamma \rightarrow \chi_{cJ} \rightarrow \pi^+\pi^-$ [2].

The general trend of the angular dependence of the differential cross section is as follows: The differential cross section has a maximum at $|\cos\theta^*| = 0$ for the $W < 2.1$ GeV region. For the $W > 1.9$ GeV, however, the angular dependence shows a rise toward the forward angles. In the higher W region, the point in c.m. angle at which the rise in the differential cross section begins moves toward the forward direction, and the rise gets steeper, as W increases.

We show the cross section ratio between $\gamma\gamma \rightarrow \pi^0\pi^0$ and $\gamma\gamma \rightarrow \pi^+\pi^-$ [2] for $|\cos\theta^*| < 0.6$ and $2.4 < W < 4.0$ GeV, in Fig. 10. The error bars in the figure are statistical only. Each measurement of the cross section has typically a 10% systematic error, partially correlated with each other for different points. Several $\gamma\gamma \rightarrow \pi^+\pi^-$ measurements above the charmonium masses have larger systematic errors, $\sim 25\%$.

The energy dependence of the ratio above $W > 2.7$ GeV is smooth with a value around 0.3-0.4. This ratio is larger than the prediction from the lowest-order QCD calculation. We,

however, need more detailed investigations of the W and angular dependences in comparison with the predictions of the QCD models to test the expected asymptotic nature.

IX. CONCLUSION

We have measured the cross section of the process $\gamma\gamma \rightarrow \pi^0\pi^0$ in the $\gamma\gamma$ c.m. energy and angular regions of $0.60 \text{ GeV} < W < 4.0 \text{ GeV}$ and $|\cos\theta^*| < 0.8$. In the cross section, several resonant structures are seen, including a statistically significant peak from the $f_0(980)$. We find that the angular dependence (forward- and/or large-angle enhancements) changes drastically at around $W = 2.0 \text{ GeV}$. The ratio of cross sections of $\gamma\gamma \rightarrow \pi^0\pi^0$ and $\gamma\gamma \rightarrow \pi^+\pi^-$ in the 3 GeV region is also obtained.

We thank the KEKB group for the excellent operation of the accelerator, the KEK cryogenics group for the efficient operation of the solenoid, and the KEK computer group and the National Institute of Informatics for valuable computing and Super-SINET network support. We acknowledge support from the Ministry of Education, Culture, Sports, Science, and Technology of Japan and the Japan Society for the Promotion of Science; the Australian Research Council and the Australian Department of Education, Science and Training; the National Natural Science Foundation of China under contract No. 10575109 and 10775142; the Department of Science and Technology of India; the BK21 program of the Ministry of Education of Korea, the CHEP SRC program and Basic Research program (grant No. R01-2005-000-10089-0) of the Korea Science and Engineering Foundation, and the Pure Basic Research Group program of the Korea Research Foundation; the Polish State Committee for Scientific Research; the Ministry of Education and Science of the Russian Federation and the Russian Federal Agency for Atomic Energy; the Slovenian Research Agency; the Swiss National Science Foundation; the National Science Council and the Ministry of Education of Taiwan; and the U.S. Department of Energy.

-
- [1] Belle Collaboration, T. Mori *et al.*, Jour. Phys. Soc. Jpn. **76**, 074102 (2007); Belle Collaboration, T. Mori *et al.*, Phys. Rev. D **75**, 051101(R) (2007).
 - [2] Belle Collaboration, H. Nakazawa *et al.*, Phys. Lett. B **615**, 39 (2005).
 - [3] Belle Collaboration, W.T. Chen *et al.*, Phys. Lett. B **651**, 15 (2007).
 - [4] Belle Collaboration, C.C. Kuo *et al.*, Phys. Lett. B **621**, 41 (2005).
 - [5] Belle Collaboration, S. Uehara *et al.*, Phys. Rev. Lett. **96**, 082003 (2006).
 - [6] S.J. Brodsky and G.P. Lepage, Phys. Rev. D **24**, 1808 (1981).
 - [7] M. Benayoun and V.L. Chernyak, Nucl. Phys. B **329**, 209 (1990); V.L. Chernyak, Phys. Lett. B **640**, 246 (2006).
 - [8] M. Diehl, P. Kroll and C. Vogt, Phys. Lett. B **532**, 99 (2002).
 - [9] JADE Collaboration, T. Oest *et al.*, Zeit. Phys. C **47**, 343 (1990);
 - [10] Crystal Ball Collaboration, H. Marsiske *et al.*, Phys. Rev. D **41**, 3324 (1990).
 - [11] S. Kurokawa and E. Kikutani, Nucl. Instr. and Meth. A **499**, 1 (2003), and other papers included in this volume.
 - [12] Belle Collaboration, A. Abashian *et al.*, Nucl. Instr. and Meth. A **479**, 117 (2002).
 - [13] A. Höcker and V. Kartvelishvili, Nucl. Instr. Meth. A **372**, 469 (1996).

- [14] S. Uehara, KEK Report 96-11 (1996).
- [15] GAMS Collaboration, D. Alde *et al.*, Eur. Phys. J. A **3**, 361 (1998).
- [16] Particle Data Group, W.-M. Yao *et al.*, J. Phys. G **33**, 1 (2006).